Article:
Salisbury, DJ, Anguelova, MD and Brooks, IM orcid.org/0000-0002-5051-1322 (2014) Global distribution and seasonal dependence of satellite-based whitecap fraction. Geophysical Research Letters, 41 (5). pp. 1616-1623. ISSN 0094-8276

https://doi.org/10.1002/2014GL059246

AGU PUBLICATIONS

Geophysical Research Letters

RESEARCH LETTER

10.1002/2014GL059246

Key Points:
- Seasonal dependence of global satellite-based whitecap fraction is presented
- Results are compared to parameterized estimates and differences quantified
- Implications of results for modeling air-sea processes are discussed

Supporting Information:
- Readme
- Figure S1

Correspondence to:
D. J. Salisbury,
eedjs@leeds.ac.uk

Citation:
Salisbury, D. J., M. D. Anguelova, and I. M. Brooks (2014), Global distribution and seasonal dependence of satellite-based whitecap fraction, *Geophys. Res. Lett.*, *41*, doi:10.1002/2014GL059246.

Received 11 JAN 2014
Accepted 29 JAN 2014
Accepted article online 4 FEB 2014

Global distribution and seasonal dependence of satellite-based whitecap fraction

Dominic J. Salisbury[1], Magdalena D. Anguelova[2], and Ian M. Brooks[1]

[1]Institute for Climate and Atmospheric Science, University of Leeds, Leeds, UK, [2]Remote Sensing Division, Naval Research Laboratory, Washington, District of Columbia, USA

Abstract We present the first study of global seasonal distributions of whitecap fraction, W, obtained from satellite-based radiometric observations. Satellite-based W incorporates variability from forcings other than wind speed and can capture differences in W in initial and late lifetime stages. The satellite-based W is more uniform latitudinally than predictions from a widely used wind speed-dependent parameterization, $W(U_{10})$, formulated from in situ observations, being on average higher than the $W(U_{10})$ predictions at low latitudes and lower at middle and high latitudes. This difference provides an explanation for the consistent geographical biases in sea spray aerosol concentration found in a number of large-scale models. Satellite estimates of W would benefit air-sea interaction and remote sensing applications that use parameterizations in terms of W such as sea spray flux, gas transfer, and surface winds.

1. Introduction

Whitecaps are the surface manifestation of bubble plumes, created when surface gravity waves break and entrain air into the water column. They enhance air-sea exchange, introducing physical processes different from those operating at the bubble-free water surface. Their surface extent provides a proxy measure for physical and chemical processes that are dependent upon wave breaking and bubbles, such as gas exchange [*Monahan and Spillane*, 1984; *Asher et al.*, 1996; *Woolf*, 2005; *Zhang*, 2012], and sea spray aerosol production [*Blanchard*, 1963; *de Leeuw et al.*, 2011].

The presence of whitecaps must be accounted for in models of the global radiation budget [*Frouin et al.*, 2001] because it increases ocean albedo [*Koepke*, 1984], in optical ocean color retrievals because it masks water-leaving radiance [*Gordon and Wang*, 1994], and in surface reflection corrections for aerosol optical depth retrievals [*Sayer et al.*, 2010]. At microwave frequencies, whitecaps have higher surface emission and brightness temperature than water [*Wentz*, 1997; *Smith*, 1988; *Rose et al.*, 2002]; this has implications for remote sensing of geophysical variables, such as the ocean surface wind vector, from satellite-borne polarimetric microwave radiometers [*Wentz*, 1997; *Yueh*, 1997; *Bettenhausen et al.*, 2006].

Wave breaking and whitecap formation are controlled to first order by the wind, and the whitecap fraction W is commonly parameterized as a function of local wind speed at a 10 m reference height, U_{10}. This approach ignores the known variability in W resulting from the influence of secondary factors such as the wave state, sea surface temperature (SST), and atmospheric stability [*Monahan and O'Muircheartaigh*, 1986; *Anguelova and Webster*, 2006; *de Leeuw et al.*, 2011; *Salisbury et al.*, 2013]. Varying wind speed exponents in different $W(U_{10})$ parameterizations may reflect variability due to secondary forcings as they can be derived under conditions of different secondary factors at the same wind speed and thus show different wind speed dependencies. However, they are often extrapolated to wind speeds far beyond those they were derived from, and since they are highly nonlinear functions, this may result in significant mean biases in regions where high winds are common, such as at high latitudes, particularly for $U_{10} \gtrsim 25$ m s^{-1} [*Holthuijsen et al.*, 2012] where there are few measurements.

To date, studies of global and seasonal distributions of whitecaps have been possible only by driving $W(U_{10})$ parameterizations with global wind distributions. *Blanchard* [1963] showed the latitudinal variation of W by estimated zonal means for June–August and December–February; these varied from a minimum of ~2% in the tropics to ~9% at 45°S during June–August. The seasonal contrast was highly asymmetric. In the Southern Hemisphere, zonal means of W in summer were roughly 2% lower than winter values across the hemisphere with W peaking at around 45°S for both seasons. In the Northern Hemisphere, there was a strong seasonal cycle; W peaked just above 8% at 55°N in winter but had a near-uniform value of about

2% across the entire hemisphere in summer. It is worth noting that these results are derived from a $W(U_{10})$ parameterization based on an extremely limited data set of just five aerial photographs of the sea surface in the Caribbean, at winds between 4 and 20 m s^{-1}.

A monthly global climatology of W was presented by *Spillane et al.* [1986], based on a rate of wind work parameterization of W and ship observations of surface wind speed and stability dependent drag coefficient. Highest W (3–4%) occurred in the North Atlantic in winter. The relatively lower values (1.5–2%) for the Southern Ocean, even during the austral winter, were attributed to undersampling of high wind conditions by the ships. At low to middle latitudes (up to 40°N and 40°S) W never exceeds 1%.

Erickson III et al. [1986] used the $W(U_{10})$ function of *Monahan and O'Muircheartaigh* [1980, hereinafter MM80] and global monthly mean winds at 5° resolution. They found a similar general seasonal distribution and also highlighted geographic regions of persistently high whitecap fraction over periods of months, such as the Indian Ocean during the monsoon season and high-latitude storm tracks.

Here we use a full year of satellite estimates of whitecap fraction to assess the spatial distribution and seasonal dependence of W. We compare this global distribution with that derived from the MM80 parameterization and discuss implications for models and retrieval algorithms.

2. Method

2.1. Data

We draw on a database of satellite-based W estimates [*Salisbury et al.*, 2013], composed of gridded (0.5° × 0.5°), global estimates of W at two microwave frequencies, 10 GHz and 37 GHz (W_{10} and W_{37}). Data for all of 2006 are used in daily format. The frequency dependence of satellite-based W estimates is useful as W_{10} and W_{37} reflect different lifetime stages of the whitecaps [*Salisbury et al.*, 2013]. It has been shown [*Anguelova and Gaiser*, 2011] that decaying foam as thin as ~1 mm can be detected at 37 GHz, while 10 GHz primarily quantifies thicker foam ($\gtrsim$4 mm), i.e., newly formed whitecaps associated with actively breaking waves. As such, individual W_{37} estimates are higher than corresponding W_{10} estimates.

The database includes U_{10} estimates from the SeaWinds microwave scatterometer on board the QuikSCAT satellite and—when a SeaWinds matchup is not available—model output from the Global Data Assimilation System. *Salisbury et al.* [2013] describe the matchup procedure and the blending of satellite and model winds. We limit the wind speeds in the analysis to $U_{10} < 30$ m s^{-1}, so as to avoid the most extreme conditions, where the satellite retrieval is poorly defined. Such cases are, however, few in number (< 0.003% of estimates) and omitting them does not affect our conclusions.

2.2. Analyses

For a given grid cell, the number of estimates of W_{10} and W_{37} varies with the number of matchups between different source measurements; for calculation of seasonal means, this number ranges from 1 to 130, with an average of 34–40 depending on the season. Latitudinal variations are presented with zonal mean profiles of whitecap fraction. Zonal means were obtained by averaging all values within each 0.5° latitude band. Seasons are defined as Northern Hemisphere spring (March–May, hereafter MAM), summer (June–August, JJA), autumn (September–November, SON), and winter (December–February, DJF).

We compare satellite-based W estimates with those predicted by the $W(U_{10})$ relationship of MM80, formulated from in situ measurements of W and U_{10}:

$$W(U_{10}) = 3.84 \times 10^{-4} U_{10}^{3.41}, \quad (1)$$

where W is in percent. The highest wind speed recorded in their source data is 16.6 m s^{-1}, and so the parameterization is strictly valid only for wind speeds below this, but it is often extrapolated to much higher wind speeds. This parameterization is largely based on whitecap data sets collected in low-latitude trade wind regions; weaker wind speed dependencies (exponents slightly greater than 2) were found for high-latitude data sets [*Monahan and O'Muircheartaigh*, 1986]. We use (1) with U_{10} values from W database to obtain W_{MM80} values matched to each W_{10} and W_{37} estimate; these were similarly averaged.

The MM80 parameterization is chosen because it is widely used, forming part of the *Monahan et al.* [1986] sea spray source function and several others adapted from it, including those of *Gong* [2003] and *Mårtensson et al.* [2003], which are used to calculate sea spray aerosol source fluxes in many aerosol and

climate models [*Spracklen et al.*, 2005; *Textor et al.*, 2006]. MM80 or similar formulations are also used in sea surface reflectance models for aerosol [*Sayer et al.*, 2010] and wind speed [*Harmel and Chami*, 2012] retrievals.

A comparison is also made between values predicted by MM80 and parameterized satellite-based W estimates obtained from the $W(U_{10})$ relationships presented in *Salisbury et al.* [2013]:

$$W_{10} = 4.60 \times 10^{-3} \times U_{10}^{2.26}; \quad 2 < U_{10} \leq 20 \text{ m s}^{-1},$$
$$W_{37} = 3.97 \times 10^{-2} \times U_{10}^{1.59}; \quad 2 < U_{10} \leq 20 \text{ m s}^{-1}, \tag{2}$$

where W is expressed in percent. These functions were obtained by fitting a power law to wind speed binned W means and are valid up to a maximum wind speed of 20 m s^{-1}. Note that although these parameterizations are in terms of U_{10} alone, the wind exponents carry information for the geographical variations of whitecap fraction because equations (2) are based on W data covering meteorological and environmental conditions over the entire globe over a full year.

3. Results and Discussion

3.1. Spatial Distribution and Seasonal Changes

The seasonal global distributions of W_{10} and W_{37} (Figure 1) follow similar patterns, with W_{37} always higher, as expected. Highest seasonal W occurs in bands centered around 50°N and 50°S, where mean wind speeds are highest [*Sayer et al.*, 2010]. The Southern Hemisphere band is persistent, with $W_{10} > 1.5\%$ and $W_{37} > 2\%$ over much of the Southern Ocean throughout the year. This feature was apparent in the monthly maps of W presented in *Spillane et al.* [1986]. Over much of the low-latitude ocean (equatorward of 30°N and 30°S), seasonal means of W_{10} are usually <0.5%, while W_{37} seasonal means are typically above 0.5%. Like *Erickson III et al.* [1986], we find enhanced W in the Arabian Sea during summer, with mean $W_{10} \approx 1.5\%$ and mean $W_{37} \approx 2\%$.

The latitudinal variation of W_{10} and W_{37} for the four seasons is shown in Figure 2, along with that for W_{MM80}. Values of W_{10} and W_{37} follow roughly the same latitudinal trends, with zonal means of W_{37} larger than those for W_{10} by a factor of 1.5–2. In the equatorial region, W_{10} is consistently around 0.3%, with W_{37} at ~0.6%. There is a general trend of increasing W from the equator to high latitudes, and a consistent asymmetry between the two hemispheres. Interseasonal variations are much stronger in the Northern Hemisphere; at 50–60°N, where W peaks, W_{10} is a factor of 3 and W_{37} a factor of approximately 2 higher in DJF than in JJA. In the Southern Hemisphere, W peaks around 50°S; here W_{10} varies less than 30% and W_{37} less than 20% over the year. This result is in agreement with the findings of *Blanchard* [1963] and *Erickson III et al.* [1986]. The asymmetric distribution in mean W is a consequence of the larger seasonal variations of temperature and winds in the Northern Hemisphere (driven by the stronger response of land surface temperature) and persistent high winds and long fetches in the Southern Ocean, both of which result from the asymmetric distribution of land masses between the hemispheres.

3.2. Comparison With In Situ $W(U_{10})$ Parameterization

Latitudinal variations of W_{10} are in close agreement with W_{MM80} at low latitudes (Figure 2). At higher latitudes (poleward of 40°N and 40°S), W_{MM80} is much larger than W_{10}, particularly so in the winter. Large differences here are driven primarily by the difference in wind speed dependence between satellite estimates ($U_{10}^{2.26}$ and $U_{10}^{1.59}$ for W_{10} and W_{37}, respectively [*Salisbury et al.*, 2013]) and MM80 ($U_{10}^{3.41}$). The extrapolation of MM80 to wind speeds beyond those from which it was formulated is likely the source of significant high bias in the resulting W estimates. Only during Northern Hemisphere summer are seasonal means of W_{10} and W_{MM80} in agreement at high latitudes. Zonal means of W_{37} are higher than W_{MM80} over much of the global ocean; the reverse is true during DJF in the high northern latitudes and in JJA around 50°S.

Aggregating individual W estimates over the full year, we compute the mean difference (MD) between W_{MM80} and both W_{10} and W_{37}, $\text{MD} = \overline{W} - \overline{W}_{\text{MM80}}$, together with the normalized mean difference (NMD), $\text{NMD} = 100 \times \text{MD}/\overline{W}_{\text{MM80}}$.

The MD between W_{MM80} and both W_{10} and W_{37} are shown in Figures 3a and 3b. Over much of the middle and lower latitudes (between 30°N and 30°S), MD is close to zero for W_{10}; for W_{37}, MD is positive and reaches 0.8% in low wind speed regions. At higher latitudes, MD increases in magnitude, reaching −2.4% in regions of the Southern Ocean for W_{10}. These are high wind speed regions, where W_{MM80} is consistently higher than W_{10}. In these regions, MD for W_{37} is generally not as large because W_{37} estimates are higher than W_{10}.

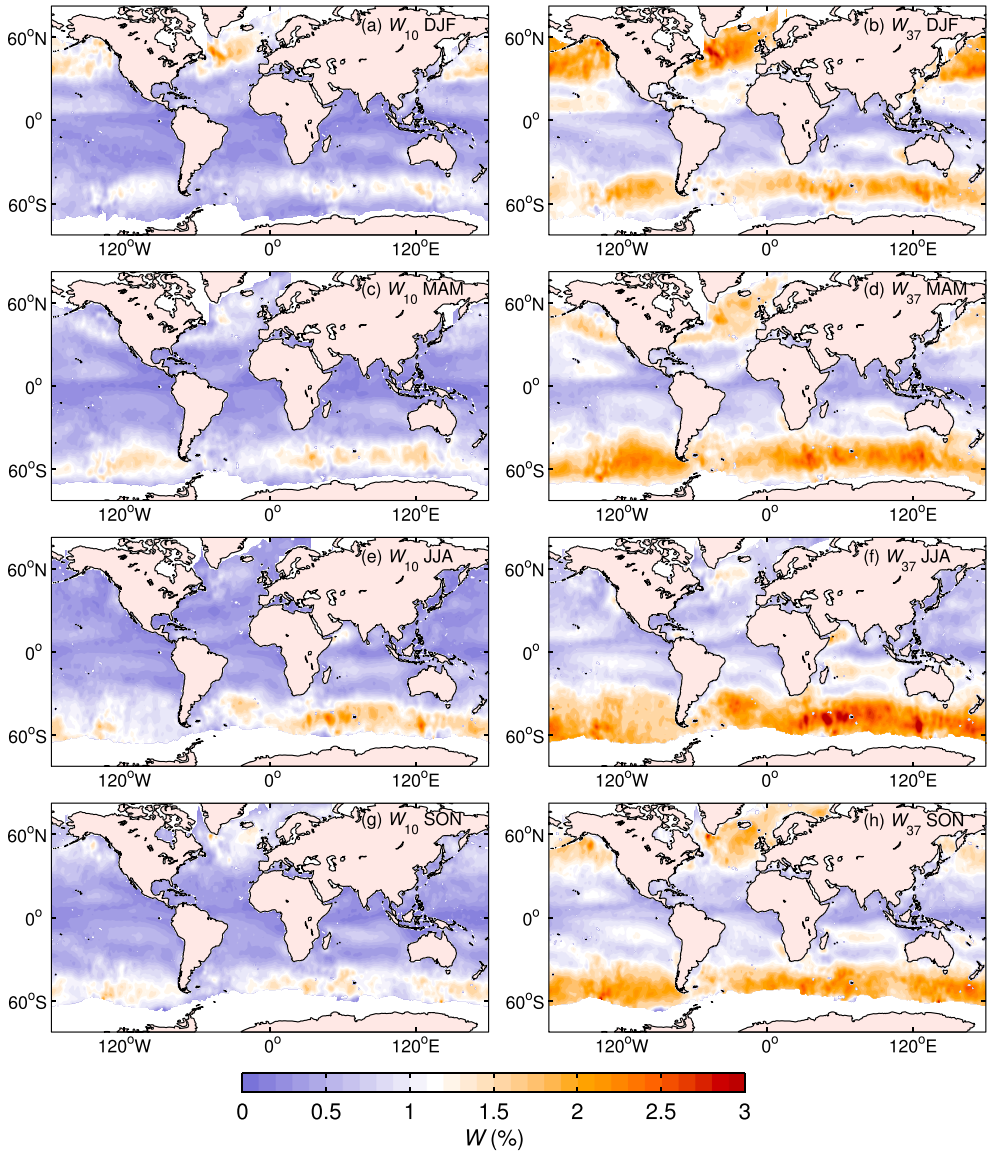

Figure 1. Seasonal means of (left) W_{10} and (right) W_{37}.

Figures 3c and 3d show normalized mean differences between W_{MM80} and W_{10} and W_{37}, respectively. NMD for W_{10} lies between −50% and 50% over much of the oceans. A somewhat different behavior is seen for W_{37}; in equatorial regions and low latitudes, NMD can be as large as 240%, reflecting the large relative difference between W_{37} and W_{MM80}. The difference between the two frequencies results from the physically different nature of the properties they respond to: the foam in actively breaking waves and the slowly decaying surface foam. This imposes both a large difference in mean W and differences in response to environmental conditions.

In the same manner, we compare W estimates predicted by MM80 with parameterized satellite-based estimates (equation (2)), rather than true satellite W estimates. The resulting MD and NMD maps (Figure S1 in the supporting information) show that the effect of using parameterized satellite-based values is small, with the ranges and spatial distributions of MD and NMD almost equivalent to those shown in Figure 3. The small differences suggest that parameterized satellite-based values of whitecap fraction differ from MM80 predictions in the same way as the direct satellite observations of W. In other words, the wind exponents in the $W(U_{10})$ parameterizations (2) capture well the geographical variability of W carried by the direct satellite observations of W.

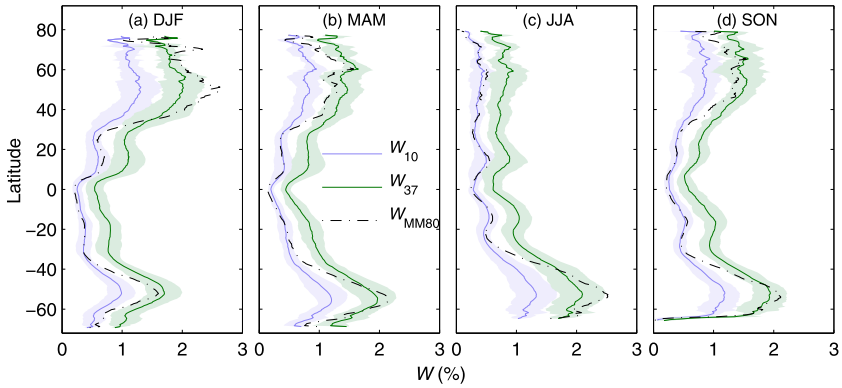

Figure 2. Latitudinal variation of seasonal means of W_{10}, W_{37}, and W_{MM80}. Shaded areas represent standard deviation on means.

3.3. Implications

In models and remote sensing applications, W is specified through use of $W(U_{10})$ parameterizations. However, these parameterizations are based on limited in situ data sets and are known to miss contributions to variability in W resulting from second-order forcings [*Salisbury et al.*, 2013].

An important application is the use of W to estimate the sea spray aerosol (SSA) source flux in aerosol and climate models. Generally, the SSA source flux is prescribed through application of the whitecap method, scaling an estimate of the production flux per unit area whitecap, often derived from laboratory measurements, by W, or by scaling a time average of this production flux by W/τ [*Monahan et al.*, 1986], where τ is a characteristic e-folding whitecap decay time. As such, any uncertainty in W transfers directly to the flux estimates. Many of the resulting sea spray source functions (SSSF) use MM80 (1), resulting in fluxes with a $U_{10}^{3.41}$ dependence. Such a dependence yields large source fluxes at high winds, resulting in modeled sea salt number and mass concentrations typically higher than those measured [*de Leeuw et al.*, 2011; *Ovadnevaite et al.*, 2012]. *Tsyro et al.* [2011] found that model estimates based on the SSSFs of *Mårtensson et al.* [2003] and *Gong* [2003] overestimate atmospheric concentrations of Na by as much as 46% compared to observations. Similarly, through a comparison of modeled and ship measured sea salt mass concentrations, *Witek et al.* [2007] found that modeled concentrations were biased high—increasingly so with U_{10}. *Jaeglé et al.* [2011] found

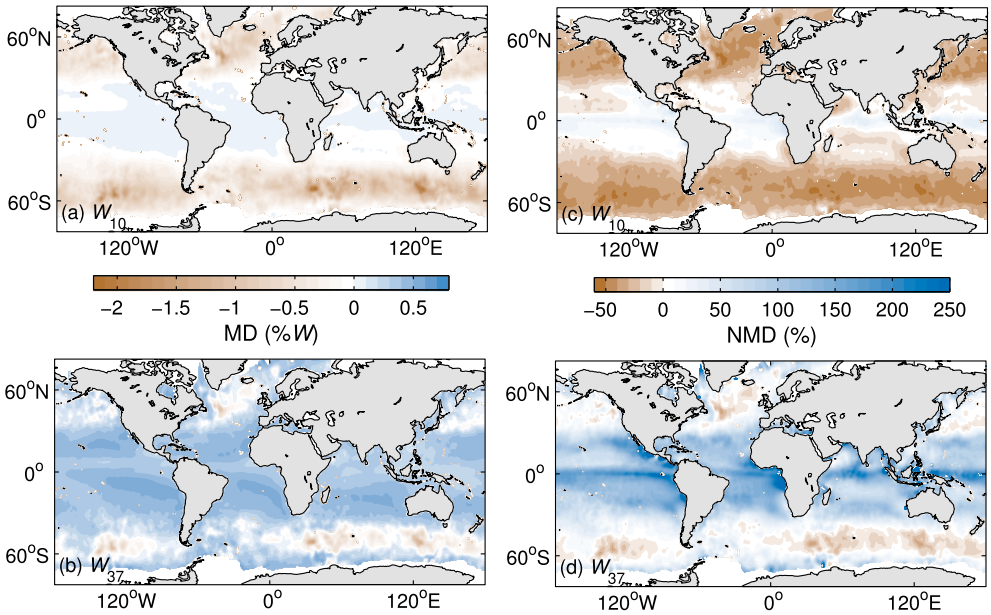

Figure 3. Mean difference (MD = $\overline{W} - \overline{W}_{MM80}$) and normalized mean difference (NMD = $100 \times \mathrm{MD}/\overline{W}_{MM80}$) between W_{MM80} and (a and c) W_{10} and (b and d) W_{37}.

that the GEOS-Chem model consistently underestimates SSA concentrations in the tropics (SST > 25°C) and overestimates at higher latitudes (SST < 10°C).

That the uncertainty of the SSA flux drives substantial geographical biases has also been noted in model estimates of derived quantities. Using a lower limit for sea salt concentrations, *Haywood et al.* [1999] could not reconcile modeled and measured values of solar irradiance. Use of higher sea salt concentrations brought balance over much of the globe but overestimation at high latitudes. Such overestimation at high latitudes for aerosol optical depth (AOD), accompanied with underestimation at low latitudes, persisted in models in which the SSSF uses the MM80 $W(U_{10})$ parametrization [*Chin et al.*, 2002]. *Smirnov et al.* [2011] found that modeled AODs south of 40°S are consistently higher than Sun photometer measurements; many of the models compared use MM80 $W(U_{10})$ parametrization as well.

Such biases in modeled sea salt concentrations and derived quantities cannot be solely attributed to biases in SSA source flux estimates; transport and removal processes also play a role, as does the quality of the wind speed data driving the parameterization. However, the geographical biases outlined above are consistent with our findings regarding the differences between MM80 and satellite retrievals of W (section 3.2). In high-latitude regions such as the North Atlantic and Southern Ocean, where mean wind speed is highest, mean W_{10} is up to 60% lower than mean W_{MM80}, while mean W_{37} is up to 40% lower. In low-latitude regions where wind speeds are consistently low, the 1 year mean of W_{10} is up to 50% larger than W_{MM80}, whereas mean W_{37} can be as much as 240% higher. As modeled SSA source fluxes scale linearly with W, use of satellite-based W estimates (either directly measured or parameterized) instead of MM80 in a SSSF would result, on average, in larger SSA fluxes in low wind speed regimes and smaller fluxes in high winds, by the factors shown in Figure 3. Because W_{10} and W_{37} capture the natural variability of whitecap formation and lifetime, our results imply that discrepancies between modeled and measured quantities can be, at least partially, reconciled with the use of satellite-based estimates of W.

With regard to the use of satellite-based estimates for obtaining SSA emissions using the whitecap method, we are not yet able to say whether W_{10}, W_{37}, or indeed some combination of both, is the most appropriate measure. One might presume W_{37} is a preferable measure, as it quantifies both active and residual whitecap stages, both of which involve bubble bursting and SSA production. However, a number of caveats hamper reliable characterization of SSA production. The relative contribution of active and residual whitecaps to total SSA production should be weighted by their respective decay times using W/τ [*Monahan et al.*, 1982, 1986], but more measurements are necessary to quantify the decay times. Different production fluxes per unit area of whitecap in active and decaying phases are expected to be necessary, since the bubble size distributions and rate of bursting will be different in each; these have not been characterized. In laboratory studies, *Woolf et al.* [1987] observed aerosol production to continue after the decay of a visible whitecap signature. This is likely the result of a small flux of bubbles small enough to remain in the water column for an extended period and which burst too rapidly at the surface for a foam layer to be maintained. Their concentration and size distribution ought, however, to be related to their rate of production and hence whitecap formation and W_{10}. Furthermore, the production flux per unit area whitecap is expected to change with the scale of individual breaking waves; recently, *Norris et al.* [2013] showed a sizeable wind speed dependence of the production flux per unit area whitecap for small particles but no distinguishable change for large particles over individual whitecaps. It is also possible that the relevance of W_{10} and W_{37} could vary with emitted SSA particle size: smaller particles (produced by film droplets) are associated with the bursting of larger bubbles which rise to the surface rapidly and are thus more concentrated in recent/active breakers; on the other hand, larger particles (produced by jet droplets) are associated with smaller bubbles which can stay mixed in surface layer much longer and may reach the surface over a longer period. Thus, W_{10} may be more relevant to the production of smaller particles, while W_{37} could be better related to production of larger particles. Finally, the stabilization of bubbles by biological surfactants is a factor known to influence foam in its decaying stage [*Callaghan et al.*, 2013] and so can be expected to affect W_{37} estimates and their SSA production rate more than the W_{10} estimates.

At this stage—based on an assumption that the currently used production rates are more likely representative of thicker active whitecaps (as quantified by W_{10}), and the closer agreement between the wind speed dependence of W_{10} and traditional parameterizations—we suggest that use of W_{10} is preferable to W_{37}.

Our discussion so far has focused on the utility of satellite-based W estimates for aerosol, climate, and chemical transport models which need to predict the SSA source flux. Satellite-based estimates of W would

also benefit modeling of other air-sea interaction processes associated with whitecaps. These include gas exchange, storm intensification, global radiation budget, and ocean albedo. It would also improve the accuracy of remote sensing retrievals of geophysical variables such as wind vector, sea surface salinity, and ocean color. Routine availability of satellite-based W estimates can facilitate further evaluation of such benefits. Thus efforts improving satellite observations of oceanic whitecaps are encouraged.

4. Conclusions

The global distribution and seasonal dependence of whitecap fraction at two microwave frequencies (W_{10} and W_{37}) have been described. Seasonal means of the two estimates have similar geographical distributions, with W_{37} seasonal means a factor 1.5–2 higher than those for W_{10}. At low latitudes (equatorward of 30°N and S), seasonal means rarely reach 1% for W_{10} and 1.5% for W_{37}. Seasonal changes in middle to high latitudes are stronger in the Northern Hemisphere than in the Southern Hemisphere; this reflects the effects of the asymmetry in distribution of continental land masses between the hemispheres. Highest seasonal W occurs in DJF in the North Atlantic and JJA Southern Ocean.

Differences between satellite-based estimates of W and those obtained from the widely used $W(U_{10})$ relationship of *Monahan and O'Muircheartaigh* [1980] are driven primarily by their differing wind speed dependence, which is weaker for the satellite-based estimates. This results in satellite estimates higher than those obtained from MM80 in the tropics but lower than MM80 in high latitudes where mean wind speeds are higher. Overestimation of MM80 due to extrapolation beyond its range of validity is likely a key bias at high wind speeds. These differences are robust if a comparison is made between MM80 W estimates and parameterized satellite-based estimates. The satellite-based parameterizations (2) are derived from W estimates on a global scale and so their wind speed dependence will in part reflect the influence of factors other than wind speed which covary with the wind geographically; for example SST, biological surfactant concentration, and fetch-dependent wave state. As the data set of satellite-based W estimates is not yet freely available for use, the satellite-based $W(U_{10})$ parameterizations can be used in lieu of observed W_{10} and W_{37} estimates.

The use of $W(U_{10})$ parameterizations based on limited in situ data can lead to biases in the global distribution of W. This in turn leads to biases in predictions of SSA source fluxes. Such biases are consistent with recent results showing both general overestimation of modeled SSA concentrations in high latitudes and underestimation in the tropics. These biases can be reduced with use of satellite-based estimates of W to estimate SSA source fluxes. An improved representation of the spatial and temporal distribution of W will also benefit parameterizations of air-sea interaction processes and accuracy of remote sensing retrievals. Routine satellite observations of whitecap fraction can provide such improved spatial and temporal distribution of W.

Acknowledgments

We express our thanks to two anonymous reviewers for helpful comments and suggestions and to the WindSat team at the Naval Research Laboratory, Washington DC. D.S. and I.M.B. are supported by NERC grant NE/H004238/1. M.D.A. is supported by the Office of Naval Research, NRL Program element 61153N, work units WU 8967 and WU 4500.

The Editor thanks two anonymous reviewers for their assistance in evaluating this paper.

References

Anguelova, M. D., and P. W. Gaiser (2011), Skin depth at microwave frequencies of sea foam layers with vertical profile of void fraction, *J. Geophys. Res.*, *116*, C11002, doi:10.1029/2011JC007372.

Anguelova, M. D., and F. Webster (2006), Whitecap coverage from satellite measurements: A first step toward modeling the variability of oceanic whitecaps, *J. Geophys. Res.*, *111*, C03017, doi:10.1029/2005JC003158.

Asher, W. E., L. M. Karle, B. J. Higgins, P. J. Farley, E. C. Monahan, and I. S. Leifer (1996), The influence of bubble plumes on air-seawater gas transfer velocities, *J. Geophys. Res.*, *101*(C5), 12,027–12,041, doi:10.1029/96JC00121.

Bettenhausen, M., C. Smith, R. Bevilacqua, N. Wang, P. Gaiser, and S. Cox (2006), A nonlinear optimization algorithm for WindSat wind vector retrievals, *IEEE Trans. Geosci. Remote Sens.*, *44*(3), 597–610, doi:10.1109/TGRS.2005.862504.

Blanchard, D. (1963), The electrification of the atmosphere by particles from bubbles in the sea, *Prog. Oceanogr.*, *1*, 73–112.

Callaghan, A. H., G. B. Deane, and D. M. Stokes (2013), Two regimes of laboratory whitecap foam decay: Bubble-plume controlled and surfactant stabilized, *J. Phys. Oceanogr.*, *43*, 1114–1126, doi:10.1175/JPO-D-12-0148.1.

Chin, M., et al. (2002), Tropospheric aerosol optical thickness from the GOCART model and comparisons with satellite and sun photometer measurements, *J. Atmos. Sci.*, *59*(3), 461–483, doi:10.1175/1520-0469(2002)059<0461:TAOTFT>2.0.CO;2.

de Leeuw, G., E. L. Andreas, M. D. Anguelova, C. W. Fairall, E. R. Lewis, C. O'Dowd, M. Schulz, and S. E. Schwartz (2011), Production flux of sea spray aerosol, *Rev. Geophys.*, *49*, RG2001, doi:10.1029/2010RG000349.

Erickson III, D. J., J. T. Merrill, and R. A. Duce (1986), Seasonal estimates of global oceanic whitecap coverage, *J. Geophys. Res.*, *91*(C11), 12,975–12,977, doi:10.1029/JC091iC11p12975.

Frouin, R., S. F. Iacobellis, and P. Y. Deschamps (2001), Influence of oceanic whitecaps on the global radiation budget, *Geophys. Res. Lett.*, *28*(8), 1523–1526, doi:10.1029/2000GL012657.

Gong, S. L. (2003), A parameterization of sea-salt aerosol source function for sub- and super-micron particles, *Global Biogeochem. Cycles*, *17*(4), 1097, doi:10.1029/2003GB002079.

Gordon, H. R., and M. Wang (1994), Influence of oceanic whitecaps on atmospheric correction of ocean-color sensors, *Appl. Opt.*, *33*(33), 7754–7763, doi:10.1364/AO.33.007754.

Harmel, T., and M. Chami (2012), Determination of sea surface wind speed using the polarimetric and multidirectional properties of satellite measurements in visible bands, *Geophys. Res. Lett.*, *39*, L19611, doi:10.1029/2012GL053508.
Haywood, J. M., V. Ramaswamy, and B. J. Soden (1999), Tropospheric aerosol climate forcing in clear-sky satellite observations over the oceans, *Science*, *283*(5406), 1299–1303, doi:10.1126/science.283.5406.1299.
Holthuijsen, L. H., M. D. Powell, and J. D. Pietrzak (2012), Wind and waves in extreme hurricanes, *J. Geophys. Res.*, *117*, C09003, doi:10.1029/2012JC007983.
Jaeglé, L., P. K. Quinn, T. S. Bates, B. Alexander, and J.-T. Lin (2011), Global distribution of sea salt aerosols: New constraints from in situ and remote sensing observations, *Atmos. Chem. Phys.*, *11*(7), 3137–3157, doi:10.5194/acp-11-3137-2011.
Koepke, P. (1984), Effective reflectance of oceanic whitecaps, *Appl. Opt.*, *23*(11), 1816–1824, doi:10.1364/AO.23.001816.
Mårtensson, E. M., E. D. Nilsson, G. de Leeuw, L. H. Cohen, and H.-C. Hansson (2003), Laboratory simulations and parameterization of the primary marine aerosol production, *J. Geophys. Res.*, *108*(D9), 4297, doi:10.1029/2002JD002263.
Monahan, E. C., and I. G. O'Muircheartaigh (1980), Optimal power-law description of oceanic whitecap coverage dependence on wind speed, *J. Phys. Oceanogr.*, *10*, 2094–2099, doi:10.1175/1520-0485(1980)010<2094:OPLDOO>2.0.CO;2.
Monahan, E. C., and I. G. O'Muircheartaigh (1986), Whitecaps and the passive remote sensing of the ocean surface, *Int. J. Remote Sens.*, *7*(5), 627–642, doi:10.1080/01431168608954716.
Monahan, E. C., and M. C. Spillane (1984), The role of oceanic whitecaps in air-sea gas exchange, in *Gas Transfer at Water Surfaces*, edited by W. Brutsaert and G. H. Jirka, pp. 495–503, D. Reidel Publishing Company, Dordrecht, Netherlands.
Monahan, E. C., K. L. Davidson, and D. E. Spiel (1982), Whitecap aerosol productivity deduced from simulation tank measurements, *J. Geophys. Res.*, *87*(C11), 8898–8904, doi:10.1029/JC087iC11p08898.
Monahan, E. C., D. E. Spiel, and K. L. Davidson (1986), A model of marine aerosol generation via whitecaps and wave disruption, in *Oceanic Whitecaps and Their Role in Air-Sea Exchange Processes*, edited by E. C. Monahan and G. Niocaill, pp. 167–174, D. Reidel Publishing Company, Dordrecht, Netherlands.
Norris, S., I. M. Brooks, B. I. Moat, M. J. Yelland, G. de Leeuw, R. W. Pascal, and B. Brooks (2013), Near-surface measurements of sea spray aerosol production over whitecaps in the open ocean, *Ocean Sci.*, *9*(1), 133–145, doi:10.5194/os-9-133-2013.
Ovadnevaite, J., D. Ceburnis, M. Canagaratna, H. Berresheim, J. Bialek, G. Martucci, D. R. Worsnop, and C. O'Dowd (2012), On the effect of wind speed on submicron sea salt mass concentrations and source fluxes, *J. Geophys. Res.*, *117*, D16201, doi:10.1029/2011JD017379.
Rose, L. A., W. E. Asher, S. C. Reising, P. W. Gaiser, K. M. St Germain, D. J. Dowgiallo, K. A. Horgan, G. Farquharson, and E. J. Knapp (2002), Radiometric measurements of the microwave emissivity of foam, *IEEE Trans. Geosci. Remote Sens.*, *40*(12), 2619–2625, doi:10.1109/TGRS.2002.807006.
Salisbury, D. J., M. D. Anguelova, and I. M. Brooks (2013), On the variability of whitecap fraction using satellite-based observations, *J. Geophys. Res. Oceans*, *118*, 6201–6222, doi:10.1002/2013JC008797.
Sayer, A. M., G. E. Thomas, and R. G. Grainger (2010), A sea surface reflectance model for (A)TSR, and application to aerosol retrievals, *Atmos. Meas. Tech.*, *3*(2), 1023–1098, doi:10.5194/amt-3-813-2010.
Smirnov, A., et al. (2011), Maritime aerosol network as a component of AERONET—First results and comparison with global aerosol models and satellite retrievals, *Atmos. Meas. Tech.*, *4*, 1–32, doi:10.5194/amt-4-583-2011.
Smith, P. (1988), The emissivity of sea foam at 19 and 37 GHz, *IEEE Trans. Geosci. Remote Sens.*, *26*(5), 541–547, doi:10.1109/36.7679.
Spillane, M. C., E. C. Monahan, P. A. Bowyer, D. M. Doyle, and P. J. Stabeno (1986), Whitecaps and global fluxes, in *Oceanic Whitecaps and Their Role in Air-Sea Exchange Processes*, edited by E. Monahan and G. Niocaill, pp. 209–218, D. Reidel Publishing Company, Dordrecht, Netherlands.
Spracklen, D. V., K. J. Pringle, K. S. Carslaw, M. P. Chipperfield, and G. W. Mann (2005), A global off-line model of size-resolved aerosol microphysics: I. Model development and prediction of aerosol properties, *Atmos. Chem. Phys.*, *5*(1), 179–215, doi:10.5194/acp-5-2227-2005.
Textor, C., et al. (2006), Analysis and quantification of the diversities of aerosol life cycles within AeroCom, *Atmos. Chem. Phys.*, *6*(7), 1777–1813, doi:10.5194/acp-6-1777-2006.
Tsyro, S., W. Aas, J. Soares, M. Sofiev, H. Berge, and G. Spindler (2011), Modelling of sea salt concentrations over Europe: Key uncertainties and comparison with observations, *Atmos. Chem. Phys.*, *11*(20), 10,367–10,388, doi:10.5194/acp-11-10367-2011.
Wentz, F. (1997), A well-calibrated ocean algorithm for special sensor microwave/imager, *J. Geophys. Res.*, *102*, 8703–8718, doi:10.1029/96JC01751.
Witek, M. L., P. J. Flatau, P. K. Quinn, and D. L. Westphal (2007), Global sea-salt modeling: Results and validation against multicampaign shipboard measurements, *J. Geophys. Res.*, *112*, D08215, doi:10.1029/2006JD007779.
Woolf, D. K. (2005), Parametrization of gas transfer velocities and sea-state-dependent wave breaking, *Tellus B*, *57*(2), 87–94, doi:10.1111/j.1600-0889.2005.00139.x.
Woolf, D. K., P. A. Bowyer, and E. C. Monahan (1987), Discriminating between the film drops and jet drops produced by a simulated whitecap, *J. Geophys. Res.*, *92*(C5), 5142–5150, doi:10.1029/JC092iC05p05142.
Yueh, S. (1997), Modeling of wind direction signals in polarimetric sea surface brightness temperatures, *IEEE Trans. Geosci. Remote Sens.*, *35*(6), 1400–1418, doi:10.1109/36.649793.
Zhang, X. (2012), Contribution to the global air–sea CO_2 exchange budget from asymmetric bubble-mediated gas transfer, *Tellus B*, *64*, 17,260, doi:10.3402/tellusb.v64i0.17260.